Journal of Catalysis **205,** 354–357 (2002)
doi:10.1006/jcat.2001.3428, available online at http://www.idealibrary.com on IDEAL®

Anomalous Small-Angle X-Ray Scattering on a New, Nonpyrophoric Raney-Type Ni Catalyst

A. Bóta,*,[1] G. Goerigk,† T. Drucker,* H.-G. Haubold,† and J. Petró*,[2]

*Institute of Physical Chemistry, Budapest University of Technology and Economics, Müegyetem rkp 3, H-1521 Budapest, Hungary; and †Institute of Solid State Physics, Research Centre Jülich, D-52425 Jülich, Germany

Received July 12, 2001; revised September 28, 2001; accepted October 1, 2001

The nickel part of a new, nonpyrophoric Raney-type catalyst was characterized by using anomalous small-angle X-ray scattering. The mean particle size distribution determined by the method as meant by C. G. Shull and L. C. Roess (*J. Appl. Phys.* 18, 295 (1947)) was in good agreement with the domain size obtained from the broadening of the (111) Bragg reflection peak of the metallic nickel using the Scherrer equation and with the size observed by TEM. Moreover, it was found that the nickel particles have a cylindrical shape and do not exhibit surface fractal behavior. © 2002 Elsevier Science

Key Words: **ASAXS; particle size distribution; Raney-type catalyst.**

INTRODUCTION

Raney-type nickel is widely used for liquid-phase hydrogenation–dehydrogenation in the fine chemical industry. A new Raney-type catalyst was developed to eliminate its pyrophority, which is the main drawback of the standard material. The activity data and the physicochemical character of the new catalyst are described in our recently published paper (1). The new catalyst can be applied in all liquid-phase hydrogenations where standard Raney Ni is used, with the same or higher specific activity. The analysis of the pore structure based on nitrogen adsorption–desorption isotherms shows that the new catalyst has a higher (by about one order of magnitude) specific surface area than that of the standard. The structure of the new catalyst has been studied by different methods (X-ray powder diffraction (XRD), small-angle X-ray scattering (SAXS), transmission electron microscopy (TEM), scanning electron microscopy (SEM)). These investigations reveal that the system consists of at least four parts: nickel, gibbsite, bayerite, and pores. It contains 25–30 w/w% of finely dispersed nickel. The wide-angle X-ray diffractogram shows that in addition to the diffraction peaks of gibbsite and bayerite, two broad peaks appear at $2\Theta = 44.5$ and 51.5°. The first was attributed to the (111) reflection of metallic nickel and was applied for the determination of the domain size by using the Scherrer equation. The mean crystallite size is 54 Å. This value agrees well with the size determined by electron microscopy (around 40 Å). However, a broad background peak extends in the range of 2Θ, from 35 up to 55°. The background correction seems to be very difficult, as the scattering originates from the multicomponent system. The activity of the catalyst depends essentially on the structural behavior, therefore the aim of the present work is the characterization of the nickel part.

Anomalous small-angle X-ray scattering (ASAXS) is an excellent method to overcome the problem of separating the small-angle scattering of the nickel part from that of the whole system (2). If the SAXS measurements are carried out at different X-ray energies, at the energies which are close to the X-ray absorption edge of the nickel, the scattering factor of the nickel can be varied. Therefore the difference of two SAXS curves is characteristic only of the nickel particles without the contribution of the other components and pores. By using the ASAXS method not only the size distribution of the nickel particles was calculated, but also their shape was determined.

EXPERIMENTAL

The new Raney-type catalyst was prepared from Ni–Al alloy powder using NaOH solution (for details see Ref. 1). The dried sample was placed into the powder sample holder covered by a Mylar foil.

The ASAXS measurements were performed on the JUSIFA small-angle scattering apparatus of the DORYS synchrotron radiation source in DESY (Hamburg) (3). For the contrast variation the SAXS curves were detected at 8037, 8323, and 8332 eV near the nickel X-ray absorption edge (at 8333 eV). The net scattering data collected at different energies were computed to the same abscissa, normalized for the primary beam intensity, and corrected for absorption. The scattering variable, h, is defined as $h = (4\pi/\lambda)\sin\Theta$, where λ is the energy-dependent wavelength, and Θ is the half-value of the scattering angle.

[1] To whom correspondence should be addressed. Fax: 00 36 1 463 3767. E-mail: bota.fkt@chem.bme.hu.

[2] To whom correspondence should be addressed. Fax: 00 36 1 463 3648.

0021-9517/02 $35.00

The TEM image was obtained with a JEOL JEM 100 (Japan) electron microscope. The electron micrograph was recorded at optimum contrast using an objective aperture with a radius of 0.7 nm in the diffraction plane.

RESULTS AND DISCUSSION

The measurement of the absorption edge of metal nickel serves for calibration of the energy adjusted by two monochromatic crystals at the JUSIFA beamline. The same measurement on the sample shows that nickel is present in the sample, and the modified absorption edge indicates some change in the chemical structure of the nickel particles. The absorption edges measured on nickel foil (99.99%) and the catalyst are shown in Fig. 1. The difference in the shape of the Ni absorption edge indicates that the structure of the nickel in the catalyst differs from that of the pure metal. Generally, the atomic scattering factors are complex quantities and energy dependent. The complex term of the scattering factor is proportional to the linear absorption coefficient, therefore its change can be followed in Fig. 1. The energy-dependent other term is real and connected to the complex term by the Kramers–Kronig relation. Taking these relations into account, three energies (8037, 8323, and 8332 eV) were chosen for the ASAXS measurements.

At all three energies intensive small-angle scattering of the sample appears, as can be seen in Fig. 2. The closer the energy applied to the Ni absorption edge, the smaller the SAXS intensity. The contribution of the real and complex terms to the scattering factor of Ni and to the effective scattering contrast yields about 10% effect. Nearly the same effects appear for both separated SAXS curves; i.e.; the difference between the SAXS curves detected at 8037 and 8323 eV and the difference between the SAXS curves detected at 8037 and 8332 eV are similar. The separated SAXS curves are also plotted in Fig. 2. The shapes of the SAXS curves and their separated forms are different, showing

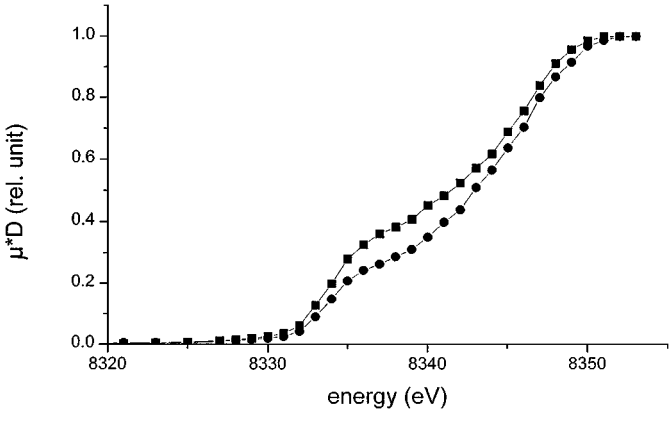

FIG. 1. Change of the linear absorption coefficient (μ) in function of the energy (E) demonstrated as μD vs E (D is the thickness of the samples, metal Ni:squares, Raney–Ni:rhombus).

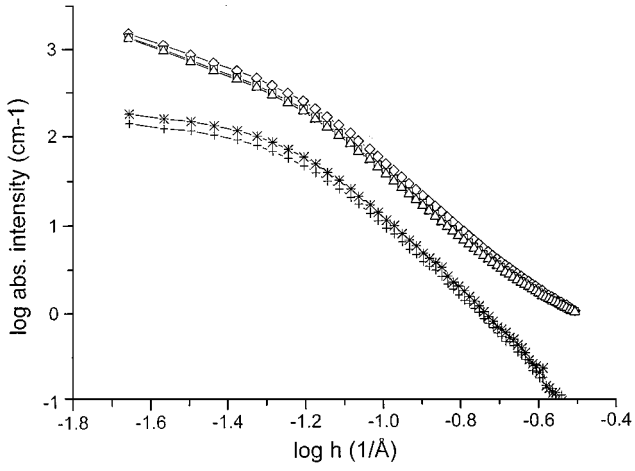

FIG. 2. ASAXS curves of the sample and their separated forms (ASAXS curves detected at $E_1 = 8037$ eV:rhombus, at $E_2 = 8323$ eV, squares; at $E_3 = 8332$ eV, triangles; separated ASAXS curves between and E_1 and E_2, cross; between E_1 and E_3, double cross.

that the contribution of the scattering of the other component is significant, and the Ni catalyst cannot be considered as a two-phase system, e.g., Ni-rich domains and matrix. The separated SAXS curves are characteristic only of the nickel particles without the contribution of the other phases present in the matrix.

The Guinier radius, R_G, can be determined from the initial section of the separated scattering curves, assuming that $R_G \cdot h < 1$, for example,

$$\log I(h) = R_G^2/3\,h^2 + \text{const}_1,$$

where $I(h)$ is the separated intensity, and const_1 is a constant. The Guinier relation is valid for monodisperse spherical structural units, but can be converted to any anisotropic form. For the new type of Ni catalyst this assumption is not fulfilled, as in the initial section of the $\log I(h)$ vs h^2 plot no straight line appears (Fig. 3). The deviation from the Guinier relation is due to the heterodispersive size distribution of the Ni particles. Shull and Roess transformed the scattering curves to obtain the parameters of various types of size distribution functions (4). If a Maxwellian-type distribution is assumed, the first part of the scattering curve can be transformed into a straight line by a fitted shift $(3/r_0^2)$ according to

$$\log I(h) = -(n+4)/2 \log\left(h^2 + 3/r_0^2\right) + \text{const}_2,$$

where r_0 and n are the parameters of the Maxwellian distribution function, and const_2 is a constant. The Maxwellian distribution is given by

$$M(R_G) = \left(2/\left(r_0^{n+1}\Gamma((n+1)/2)\right)\right) r^n \exp\left(-R_G^2/r_0^2\right),$$

where $\Gamma((n+1)/2)$ is the gamma function, and $M(R_G)$ is normalized to the total mass of the scattering particles.

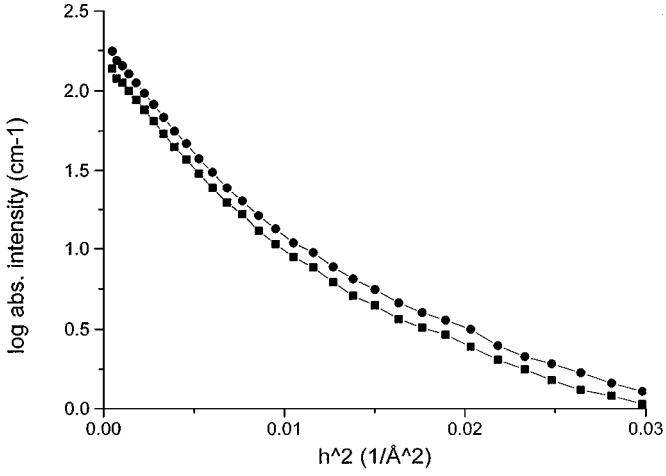

FIG. 3. Guinier plot of the separated ASAXS curves (between ASAXS (E_1) and ASAXS (E_2), squares; between ASAXS (E_1) and ASAXS (E_3), circles).

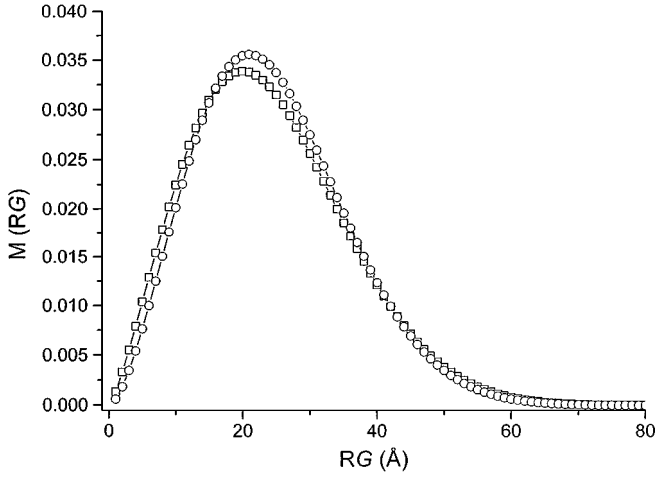

FIG. 5. Maxwellian distribution of the nickel particles of the catalyst (obtained from separated ASAXS curves).

The log $I(h)$ vs log h^2 plots have declining sections as can be seen in Fig. 4. After the linearization the best fits provide the values of r_0 (23.57, 24.99) and n (1.594, 1.286) for the two independent separate curves. The Maxwellian-type size distribution functions are plotted in Fig. 5. The difference of the two independent distributions represents the error of the size analysis obtained by ASAXS, which is 5%, and the characteristic Guinier radii are 20.0 and 21.0 Å.

If it is assumed that the shapes of the Ni particles are anisotropic, e.g., cylindrical or disk -shaped, the characteristic radius of gyration can also be observed in a $\log(h \cdot I)$ vs h^2, or $\log(h^2 \cdot I)$ vs h^2 plot, respectively. In themselves, the scattering curves do not give unambiguous information about the type of the shape of the scattering units. In the TEM images anisotropic particles can be observed which have cylindrical forms (Fig. 6). As the Ni particles have the highest electron density, we can assume that the "worm-like" units appearing in the pictures are the Ni particles. The size of particles can be estimated to be 3–4 nm. The radius of gyration of the cross section, R_{oc}, was found from the slope of the straight line in the $\log(h \cdot I)$ vs h^2 plot valid for cylindrical particles as 12.5 Å (the radius, R is $\sqrt{2}R_{oc} =$ 17.7 Å) (5). The $\log(h \cdot I)$ vs h^2 plot is shown in Fig. 7. For the cylindrical shape, its height, H, is given by

$$H^2 = 12\left(R_{Gm}^2 - R_{oc}^2\right),$$

where R_{Gm} is the mean value of the Guinier radius (20.5 Å), and a value of 56.3 Å is obtained for H. These stocky shapes can also be observed in the TEM picture (Fig. 6).

SAXS patterns provide an excellent possibility to follow the fractal behavior of the scattering system (6, 7). Both the mass and the surface fractal dimensions, D_m and D_s, can be computed if linear ranges exist in the log I vs log h plot in the medium h regime for D_m and in the Porod regime (the final section of the scattering curve) for D_s.

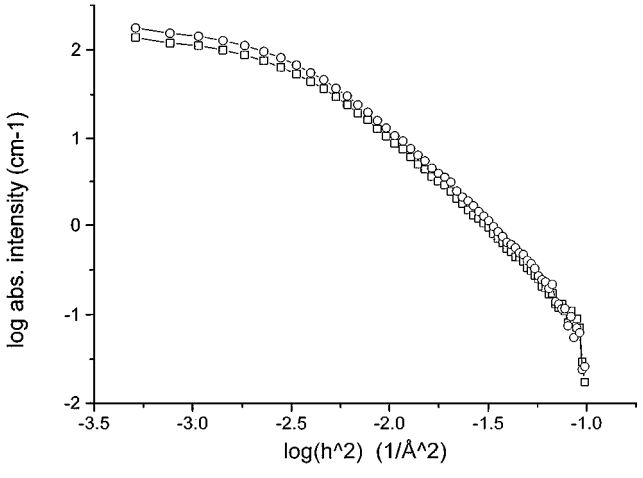

FIG. 4. Log intensity (separated ASAXS intensity between ASAXS (E_1) and ASAXS (E_2), squares; between ASAXS (E_1) and ASAXS (E_3), circles) vs log(h^2) plot for the determination of the parameters of the Maxwellian-type size distribution.

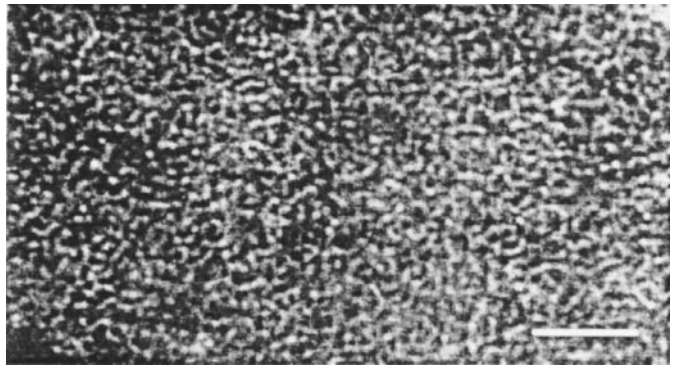

FIG. 6. TEM picture of the catalyst. (The bar represents 40 nm.)

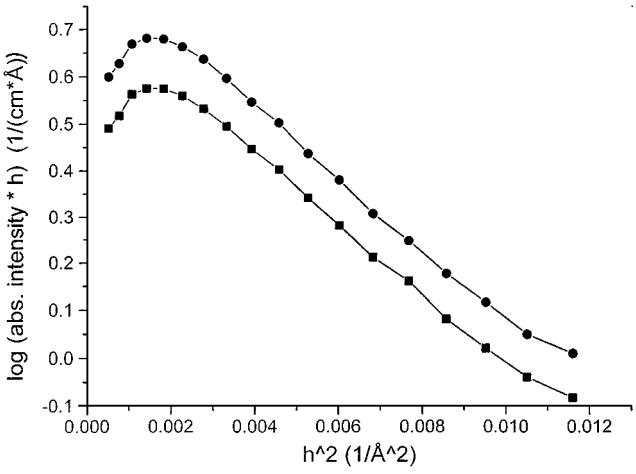

FIG. 7. Plot for the determination of the gyration of the cross section R_{oc} (obtained from separated ASAXS curves between ASAXS (E_1) and ASAXS (E_2), squares; between ASAXS (E_1) and ASAXS (E_3), circles).

The relationship between the scattering intensity and the surface fractal dimension in the larger regime of the scattering variable is given as

$$I(h) \propto h^{-6+D_s}.$$

In the medial section of the scattering curve the relationship between the scattering intensity and the mass fractal dimension is given as

$$I(h) \propto h^{-D_m}.$$

D_s and D_m fractal dimensions have the following limits: $2 \le D_s \le 3$ and $0 \le D_m \le 3$. The restriction for the determination of the mass fractal dimension is not fulfilled in our case, because no linear section exists in the $\log I$ vs $\log h$ plot as can be seen in Fig. 2. In the Porod regime the slope is 4.1 ± 0.1 showing that the Ni particles exhibit no surface fractal behavior and have a smooth surface, which means that the Ni particles are well dispersed in the solid matrix and do not form closed aggregates.

ACKNOWLEDGMENT

This work was supported by the Hungarian Scientific Funds OTKA (T 25389, Petró; and T 21781, Bóta) and a DESY-Project (Bota/Haubold II-00-060)).

REFERENCES

1. Petró, J., Bóta, A., László, K., Beyer, H., Kálmán, E., and Dódony, I., *Appl. Catal. A* **190**, 73 (2000).
2. Rasmussen, F. B., Molenbroek, A. M., Clausen, B. S., and Feidenhans, R., *J. Catal.* **190**, 205 (2000), doi:10.1006/jcat.1999.2758.
3. Haubold, H.-G., Gruenhagen, K., Wagener, M., Jungbluth, H., Heer, H., Pfeil, A., Rongen, H., Brandenburg, G., Moeller, R., Matzerath, J., Hiller, P., and Halling, H., *Rev. Sci. Instrum.* **60**, 1943 (1989).
4. Shull, C. G., and Roess, L. C., *J. Appl. Phys.* **18**, 295 (1947).
5. Kakudo, M., and Kasai, N., "X-Ray Diffraction by Polymers," p. 401. Kodansha Ltd., Tokyo, 1972.
6. Reich, M. H., Russo, S. P., Snook, I. K., and Wagenfeld, H. K., *J. Colloid Interface Sci.* **135**, 353 (1990).
7. Snook, I. K., and McMahon, P., *Langmuir* **9**, 2726 (1993).